Supporting Information

Convenient large-area construction of flexible multicolor polymer-based room temperature phosphorescence materials with second-scale phosphorescence lifetimes

Tianyu Li, †[a] Yan Zhu, †[a] Shaochen Sun,[a] Yutong Zhou,[a] Zhihui Wang,[a] Fei Li,[b] Farong Tao,*[a] Liping Wang[a] and Guang Li*[a]

[a] *School of Materials Science and Engineering, Liaocheng University, Liaocheng 252059, China*
[b] *College of Chemistry, Chemical Engineering and Materials Science, Shandong Normal University, Jinan 250014, China*
† Tianyu Li and Yan Zhu contributed equally to this work.
E-mail: taofarong@lcu.edu.cn, lglzsd@126.com

1 Experimental Section

Materials: Acrylamide (AM, 99%) was purchased from Tianjin Kemio Chemical Reagent Co., Ltd (Tianjin, China). 4-Vinylbenzyl chloride (98%) was supplied by J&K scientific Co., Ltd (Beijing, China). Fluorescein (FL, 90%) was obtained from Sinopharm Chemical Reagent Co., Ltd (Shanghai, China). Carbazole (97%), sodium alginate (SA), calcein (CAL, mixture of isomers), rhodamine 6G (R6G, 95%), sulforhodamine B (SRB, 85%) and N-vinylpyrrolidone (VP, 99%) were purchased from Shanghai Aladdin Biochemical Technology Co., Ltd (Shanghai, China). PVA-117 was provided by Kuraray Co., Ltd (Tokyo, Japan). Methacrylic acid (MMA, 99%) and vinyl acetate (VAc, 98%) were supplied from Shanghai Macklin Biochemical Technology Co., Ltd. (Shanghai, China). All other chemicals were commercially available and used as received.

Synthesis of 9-(4-vinylbenzyl)-9H-carbazole (VBC): Potassium hydroxide powder (0.45 g) was added to a stirred solution of carbazole (0.5 g) in DMSO (8 mL) at room temperature. A DMSO solution (2 mL) of 4-vinylbenzyl chloride (0.5672 g) was then added dropwise, and the mixture was stirred at room temperature for 24 h. The reaction mixture was precipitated in water, followed by filtration. The filter cake was rinsed three times with 100 mL of water and dried in an oven at 60 ^{o}C for 8 h. Finally, the crude product was purified by silica gel column chromatography using chloroform/petroleum ether (4:1, v/v) as the eluent to afford a white solid product VBC (Yield: 82.63%). ^{1}H NMR (400 MHz, $CDCl_3$, δ): 8.13 (d, J = 6.2 Hz, 2H, ArH), 7.42 (t, J = 6.2 Hz, 2H, ArH), 7.35 (d, J = 6.4 Hz, 2H, ArH), 7.29-7.23 (m, 4H, ArH), 7.09 (d, J = 6.4 Hz, 2H, ArH), 6.64

(dd, J = 8.8, 14.0 Hz, 1H, -CH=), 5.67 (d, J = 14.0 Hz, 1H, -CH_2), 5.50 (s, 2H, -CH_2-), 5.20 (d, J = 8.8 Hz, 1H, -CH_2); ^{13}C NMR (100 MHz, $CDCl_3$, δ): 140.65, 136.90, 136.73, 136.30, 126.64, 126.62, 125.88, 123.06, 120.43, 119.26, 113.96, 108.90, 46.38; HRMS (ESI) m/z: $[M + H]^+$ calcd for $C_{21}H_{18}N$, 284.1439; found, 284.1438.

Synthesis of P(AM-co-VBC): AM (2.0 g), VBC (19.3 mg) and AIBN (9.2 mg) were combined in DMF (8 mL). The mixture was stirred at 80 °C for 12 h under a nitrogen atmosphere. The resulting mixture was then cooled to room temperature and precipitated in methanol for three times. After filtration and drying in a vacuum oven at room temperature for 24 h, a white powder product P(AM-*co*-VBC) with AM/VBC feed molar ratio of 400:1 was obtained. According to the same procedure, P(AM-*co*-VBC) with other feed molar ratios of AM/VBC were synthesized. To ensure reproducibility, each batch of copolymer with a specific composition was synthesized under identical experimental conditions and repeated at least three times.

Preparation of W-P(AM-co-VBC): 50.0 mg of P(AM-*co*-VBC) with different AM/VBC feed molar ratios were dissolved in 2 mL of water and stirred for 10 min at room temperature. After that, the solutions were dried in an oven at 120 °C for 5 h, and W-P(AM-*co*-VBC) solids with varying AM/VBC ratios were obtained.

Synthesis of P(MMA-co-VBC): MMA (1.36 g), VBC (9.7 mg) and AIBN (4.6 mg) were combined in 1,4-dioxane (4 mL). The mixture was stirred at 80 °C for 12 h under a nitrogen atmosphere. After cooling to room temperature, the resulting mixture was precipitated in methanol. The resulting precipitate was filtered and dried in a vacuum oven at room temperature for 24 h, yielding a white powder product P(MMA-*co*-VBC) with MMA/VBC feed molar ratio of 400:1 (M_n = 28850, PDI = 1.48).

Synthesis of P(VP-co-VBC): VP (1.51 g), VBC (9.7 mg) and AIBN (4.6 mg) were combined in ethanol (4 mL). The mixture was stirred at 75 °C for 12 h under a nitrogen atmosphere. After cooling to room temperature, the resulting mixture was precipitated in petroleum ether. The resulting precipitate was filtered and dried in a vacuum oven at room temperature for 24 h, yielding a white powder product P(VP-*co*-VBC) with VP/VBC feed molar ratio of 400:1 (M_n = 19000, PDI = 1.89).

Preparation of W-P(VP-co-VBC): 50.0 mg of P(VP-*co*-VBC) was dissolved in 2 mL of water and stirred for 10 min at room temperature. The resulting solution was then dried in an oven at 120 °C for 5 h to afford the solid product W-P(VP-*co*-VBC).

Synthesis of P(VA-co-VBC): VAc (2.5 g), VBC (19.4 mg) and AIBN (25.2 mg) were dissolved in methanol (2.5 mL). The mixture was stirred at 65 °C for 48 h under a nitrogen atmosphere. After cooling to room temperature, the resulting mixture was precipitated in water. The precipitate was collected by filtration and dried in an oven at 80 °C for 24 h, yielding a white powder product P(VAc-*co*-VBC). Subsequently, P(VAc-co-VBC) (0.8 g) was dissolved in methanol (9 mL) and stirred at 45°C for 1 h. Then, 5% NaOH solution in methanol (0.2 mL) was added, and the reaction was continued at 45°C for 2 h. An additional 0.2 mL of 5% NaOH solution in methanol was added, and the temperature was raised from 45°C to 65°C and maintained for 2 h. After cooling to room temperature, the pH of the resulting solution was adjusted to ≤ 7 with dilute hydrochloric acid. The mixture was subjected to vacuum filtration, and the collected solid was dried in a vacuum oven at room temperature for 30 h to afford a pale yellow powder of P(VA-*co*-VBC) with VA/VBC molar ratio of 400:1. (M_n = 26590, PDI = 1.78)

Preparation of W-P(VA-co-VBC): 50.0 mg of P(VA-*co*-VBC) was dissolved in 2 mL of water and stirred for 10 min at room temperature. After that, the solution was dried in an oven at 120 °C for 5 h to afford the solid product W-P(VA-*co*-VBC).

Preparation of W-P(AM-co-VBC)/CAL composites: A 1 mL aqueous solution of CAL (0.033 mg) was added dropwise to a stirred 2 mL aqueous solution of P(AM-*co*-VBC) (50 mg) at room temperature. After stirring for 5 min, the mixture was dried at 120 °C for 5 h to give W-P(AM-*co*-VBC)/CAL solid with P(AM-*co*-VBC)/CAL weight ratio of 1000:0.66. W-P(AM-*co*-VBC)/CAL with other weight ratios of P(AM-*co*-VBC)/CAL were prepared in the same way.

Preparation of W-P(AM-co-VBC)/SRB and W-P(AM-co-VBC)/R6G composites: W-P(AM-*co*-VBC)/SRB and W-P(AM-*co*-VBC)/R6G with varying weight ratios of P(AM-*co*-VBC) to the doped fluorescent dyes were prepared following the procedure similar to that used for W-P(AM-*co*-VBC)/CAL.

Preparation of W-P(AM-co-VBC)/FL composites: A 1 mL ethanol solution of FL (0.0175 mg) was added dropwise to a stirred 2 mL aqueous solution of P(AM-*co*-VBC) (50 mg) at room temperature. After stirring for 5 min, the solution was oven-dried at 120 °C for 5 h to afford W-

P(AM-*co*-VBC)/FL solid with P(AM-*co*-VBC)/FL weight ratio of 1000:0.35. W-P(AM-*co*-VBC)/FL with other weight ratios of P(AM-*co*-VBC)/FL were prepared in the same way.

Construction of flexible multicolor RTP films: SA (0.5 g) and PVA (10.0 mg) were dissolved in deionized water (20 mL) at 90 °C, followed by dropwise addition of a 2 mL aqueous solution of P(AM-*co*-VBC) (50 mg). The mixture was stirred at 90 °C for 10 min, and then defoamed by standing at room temperature. The resulting solution was coated on a glass plate using a coating machine. After drying in an oven at 80 °C for 12 h, SA/PVA/W-P(AM-*co*-VBC) film with SA/PVA/P(AM-*co*-VBC) weight ratio of 500:10:50 was obtained. Other films of SA/ PVA/W-P(AM-*co*-VBC)/CAL with SA/PVA/P(AM-*co*-VBC)/CAL weight ratio of 500:10:50:0.4, SA/PVA/W-P(AM-*co*-VBC)/FL with SA/PVA/P(AM-*co*-VBC)/FL weight ratio of 500:10:50:0.1, SA/PVA/W-P(AM-*co*-VBC)/R6G with SA/PVA/P(AM-*co*-VBC)/R6G weight ratio of 500:10:50:0.28, and SA/PVA/W-P(AM-*co*-VBC)/SRB with SA/PVA/P(AM-*co*-VBC)/SRB weight ratio of 500:10:50:0.2 were constructed by the similar procedure as the preparation of SA/PVA/W-P(AM-*co*-VBC).

Characterization: ^{1}H NMR (500 MHz) and ^{13}C NMR (100 MHz) spectra were recorded on a Bruker AVANCE NEO 500 MHz spectrometer using $CDCl_3$ as the solvent. The HRMS spectral analysis was performed on an LTQ-Orbitrap mass spectrometer. The number-average molecular weight (M_n) and polydispersity index (PDI) of P(AM-*co*-VBC), P(VA-*co*-VBC), P(VP-*co*-VBC), were determined by an aqueous gel permeation chromatography (Breeze, Waters, USA) using 0.1 mol·L^{-1} $NaNO_3$ aqueous solution (0.8 mL/min) as the eluent and pullulan standards for calibration. The number-average molecular weight (M_n) and polydispersity index (PDI) of P(MMA-*co*-VBC) were measured by a gel permeation chromatography (Breeze, Waters, USA) using THF as the eluent and polystyrene standards for calibration. Dynamic Light Scattering (DLS) measurements were conducted using a Malvern Instruments Zetasizer Nano ZS instrument at 25 °C. The differential scanning calorimetry (DSC) was carried out on a TA25 instrument with a heating rate of 10 °C·min^{-1} under a nitrogen atmosphere.UV-Vis absorption spectra and transmittance were recorded on a Shimadzu UV-3600 spctrophotometer at room temperature. Emission spectra and time-resolved emission decay curves were acquired using an Edinburgh FS5 spectrofluorometer at room temperature. Quantum yields (QYs) were measured using the Edinburgh FS5 spectrofluorometer equipped with an integrating sphere at room temperature.

Tensile properties of the prepared films with a thickness of about 20 μm were determined using an MTS E44 universal testing machine with a crosshead speed of 0.20 mm/s. The surface morphology of the composites was characterized by field emission scanning electron microscopy (FESEM, Zeiss Ultra 55 apparatus) with an accelerating voltage of 5 kV.

Theoretical calculations: The electron density distributions of the highest occupied molecular orbital (HOMO) and lowest unoccupied molecular orbital (LUMO), along with electrostatic potential (ESP) maps, were calculated using Gaussian 09 program. The ground-state geometry optimizations were performed at the B3LYP/6-31G(d) level. Time-dependent density functional theory (TD-DFT) calculations were carried out using ORCA 5.0.4 package, and the singlet-triplet energy gap (ΔE_{ST}) and spin-orbit coupling (SOC) constants were evaluated at the level of PBE0/def2-SV(P).

2 Additional Characterization

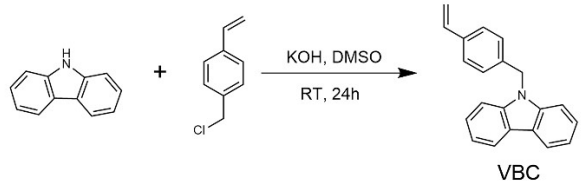

Scheme S1. Synthetic route of the monomer VBC.

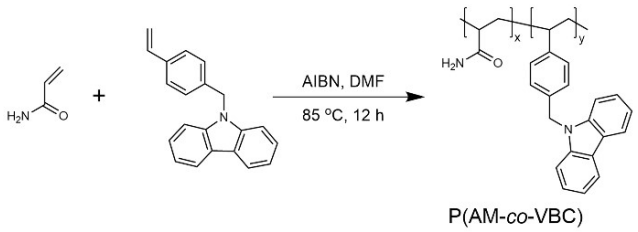

Scheme S2. Synthetic route of the copolymer P(AM-*co*-VBC).

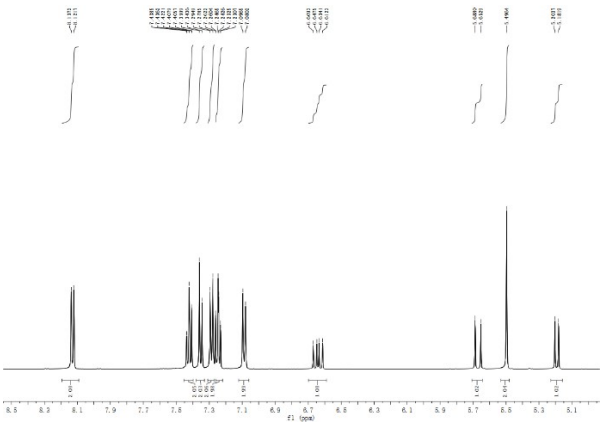

Fig. S1. ^{1}H NMR spectrum of VBC in $CDCl_3$.

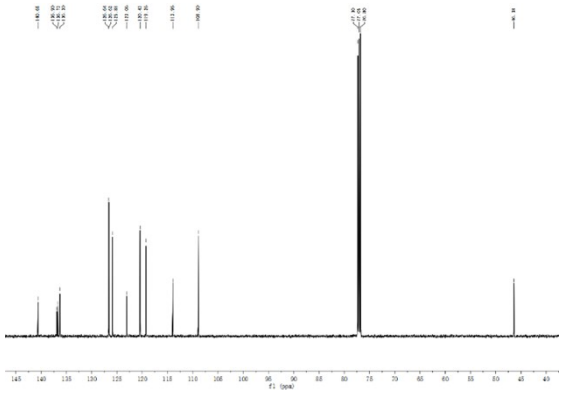

Fig. S2. ^{13}C NMR spectrum of VBC in $CDCl_3$.

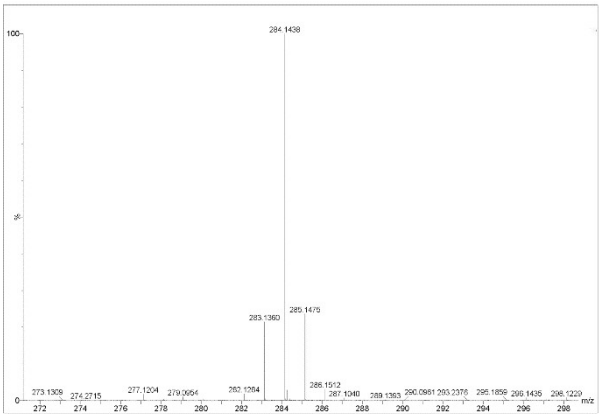

Fig. S3. HRMS spectrum of VBC.

Table S1. The relative number-average molecular weight (M_n) and polydispersity index (PDI) of P(AM-*co*-VBC).

AM/VBC feed molar ratio	M_n	PDI
100:1	7280	2.57
200:1	9620	3.06
300:1	9710	3.96
400:1	12100	4.41
500:1	11780	3.83
600:1	13630	4.40

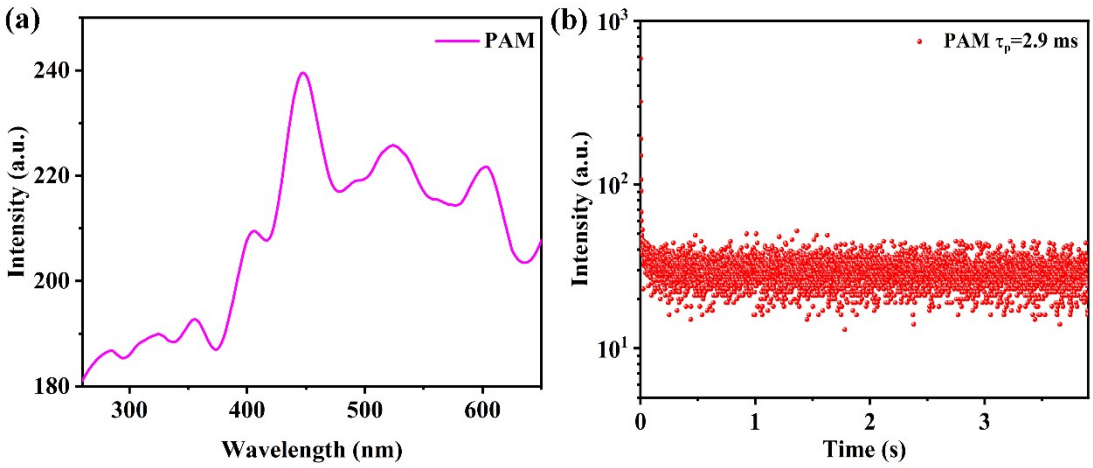

Fig. S4. (a) Phosphorescence spectrum of PAM. (b) Time-resolved decay curves of PAM.

Table S2. Photoluminescence and phosphorescence quantum yields (QYs) of P(AM-*co*-VBC).

AM/VBC feed molar ratio	QY_{PL} (%)	QY_{Phos} (%)
100:1	36.82	9.89
200:1	41.43	10.60
300:1	43.57	11.29
400:1	42.21	10.28
500:1	39.75	9.41
600:1	3.99	1.32

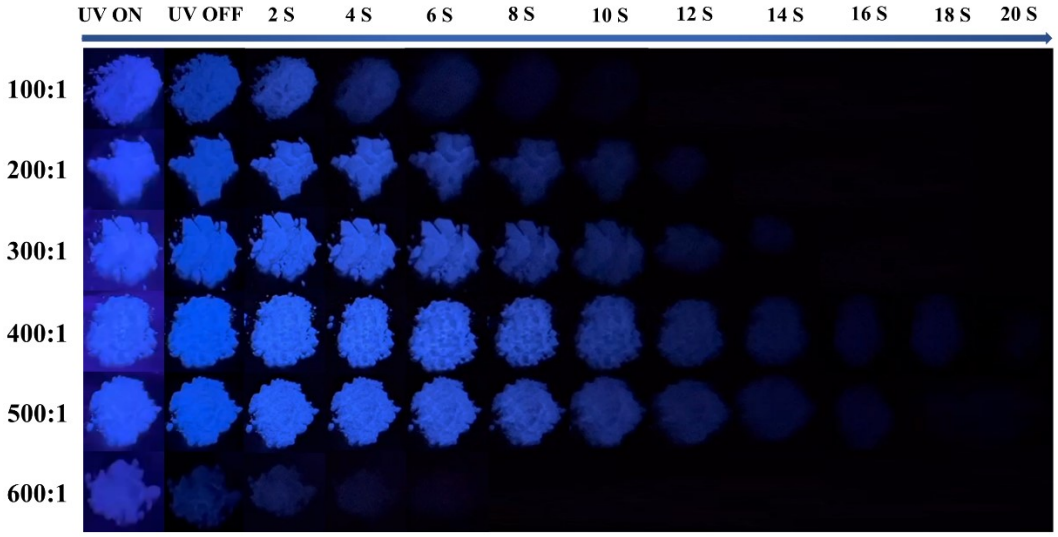

Fig. S5. Photographs of P(AM-*co*-VBC) under 254 nm UV light and after ceasing the irradiation.

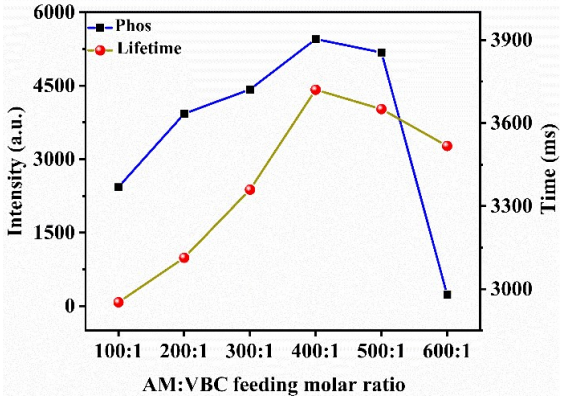

Fig. S6. The variation trend of phosphorescence intensity and lifetime of P(AM-*co*-VBC) with different feed molar ratios of AM/VBC at 442 nm.

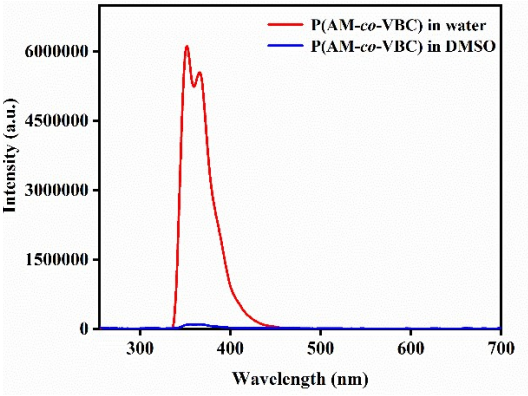

Fig. S7. (a) Steady-state PL spectrum of P(AM-*co*-VBC) with AM/VBC feed molar ratio of 400:1 in water and DMSO.

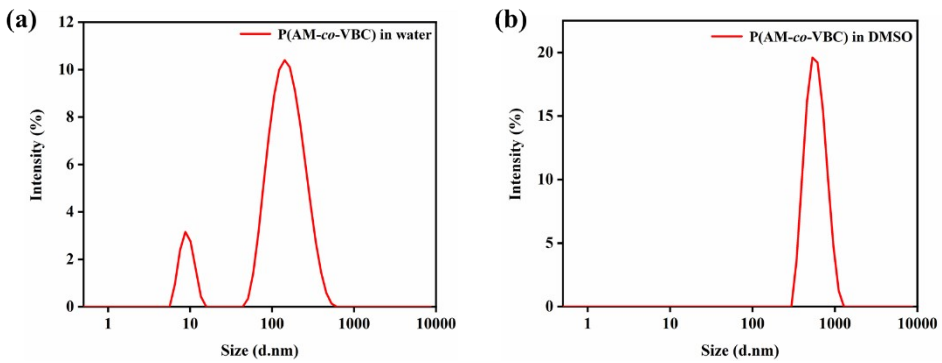

Fig. S8. Hydrodynamic diameter of P(AM-*co*-VBC) with AM/VBC feed molar ratio of 400:1 in water (a) and DMSO (b) from DLS.

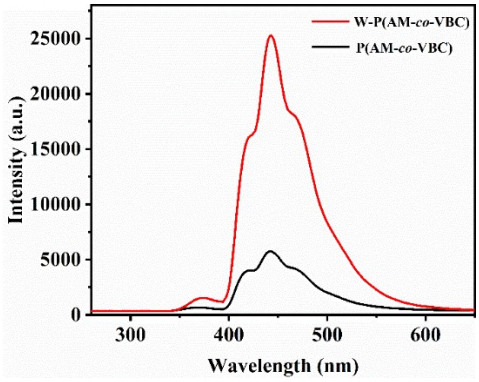

Fig. S9. Phosphorescence spectra of W-P(AM-*co*-VBC) and P(AM-*co*-VBC) with AM/VBC feed molar ratio of 400:1 (λ_{ex} = 245 nm).

Table S3. Photoluminescence and phosphorescence QYs of W-P(AM-*co*-VBC).

molar ratio	QY_{PL} (%)	QY_{Phos} (%)
100:1	29.62	13.70
200:1	41.31	16.79
300:1	46.83	19.55
400:1	59.28	24.63
500:1	49.63	20.37
600:1	5.58	3.04

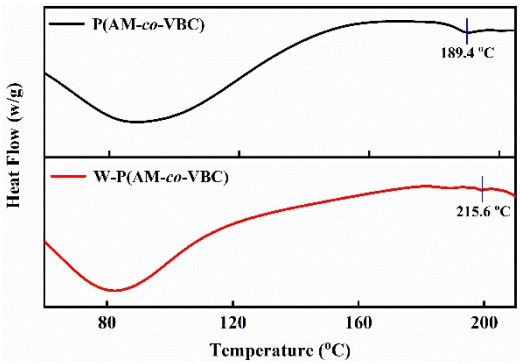

Fig. S10. DSC curves of P(AM-*co*-VBC) and W-P(AM-*co*-VBC) with AM/VBC feed molar ratio of 400:1.

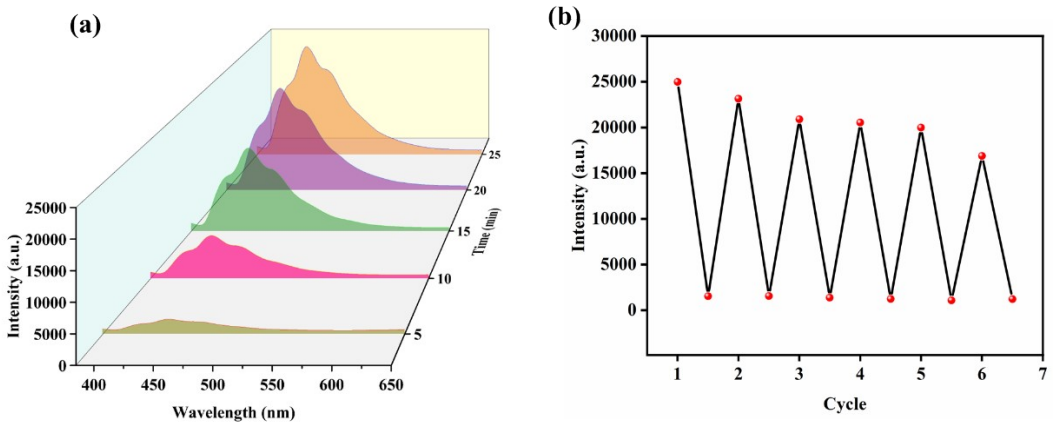

Fig. S11. (a) Phosphorescence spectra of W-P(AM-*co*-VBC) heated at 120 °C for different times. (b) RTP intensity of W-P(AM-*co*-VBC) at 442 nm upon alternating treatment of water vapor fumigation and heating.

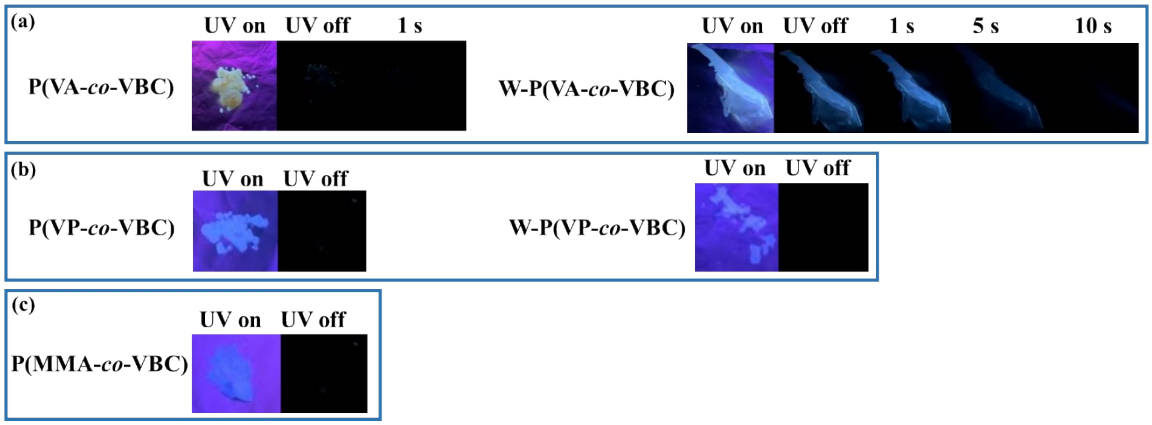

Fig. S12. Photographs of P(VA-*co*-VBC) and W-P(VA-*co*-VBC) (a), P(VP-*co*-VBC) and W-P(VP-*co*-VBC) (b), and P(MMA-*co*-VBC) (c) with a feed molar ratio of 400:1 under 254 nm UV light and after ceasing the irradiation.

Table S4. The corresponding spin-orbit coupling constants of isolated BC and BC dimer.

	Isolated BC	BC dimer	BC dimer
$\zeta(T_1\text{-}S_0)$ (cm^{-1})	0.030	0.391	0.448
$\zeta(S_1\text{-}T_1)$ (cm^{-1})	0.030	0.396	0.985
$\zeta(S_1\text{-}T_2)$ (cm^{-1})	0.033	0.717	0.197
$\zeta(S_1\text{-}T_3)$ (cm^{-1})	0.037	0.368	0.304
$\zeta(S_1\text{-}T_4)$ (cm^{-1})	0.079	0.487	0.418
$\zeta(S_1\text{-}T_5)$ (cm^{-1})	0.037	0.481	0.767
$\zeta(S_1\text{-}T_6)$ (cm^{-1})	0.022	0.136	0.881
$\zeta(S_1\text{-}T_7)$ (cm^{-1})	0.086	0.265	0.397
$\zeta(S_1\text{-}T_8)$ (cm^{-1})	0.041	0.190	0.119
$\zeta(S_1\text{-}T_9)$ (cm^{-1})	0.088	0.243	0.266
$\zeta(S_1\text{-}T_{10})$ (cm^{-1})	0.122	0.233	0.070

Table S5. The singlet (S_1) and triplet (T_n) state transition configurations for the Isolated BC.

States	Energy (eV)	Transition configuration (%)
S_1	4.158	H→L 91.7%
T_1	3.087	H-5→L+5 4.16%, H-4→L 1.58%, H-4→L+4 1.37%, H-3→L 1.18%, H-2→L+5 2.91%, H-2→L+4 1.25%, H-1→L 67.1%, H-1→L+4 1.19%, H→L+3 14.7%
T_2	3.376	H-5→L 1.56%, H-4→L+3 18.7%, H-3→L+3 1.13%, H-2→L+3 2.01%, H→L 88.3%, H→L+3 1.43%
T_3	3.607	H-4→L 2.39%, H-4→L+2 20.7%, H-3→L+1 36.7%, H-2→L+1 11.4%, H-2→L+2 22.5%
T_4	4.055	H-4→L 3.80%, H-4→L+4 1.70%, H-3→L 2.29%, H-3→L+4 1.01%, H-2→L 4.09%, H-2→L+4 1.72%, H-1→L 26.6%, H→L+3 54.6%
T_5	4.113	H-5→L 13.9%, H-4→L+3 6.27%, H-4→L+4 3.78%, H-2→L+3 6.80%, H-1→L+1 1.14%, H-1→L+3 3.95%, H-1→L +5 13.1%, H→L 7.20%, H→L+4 37.9%

T_6	4.581	H-5→L 12.7%, H-5→L+4 1.27%, H-1→L+3 79.4%, H-1→L+5 3.29%
T_7	4.609	H-5→L+3 1.56%, H-4→L 13.3%, H-3→L 9.11%, H-2→L 20.1%, H-1→L+4 9.00%, H→L+1 21.8%, H→L+3 4.60%, H→L+5 15.9%
T_8	4.707	H-4→L 1.30%, H-4→L+1 5.63%, H-4→L+2 17.5%, H-3→L+1 9.50%, H-3→L+2 8.84%, H-2→L 2.01%, H-2→L +1 34.1%, H-2→L+2 8.03%, H-1→L+4 1.15%, H→L+1 5.52%, H→L+3 1.23%, H→L+5 1.08%
T_9	4.724	H-4→L+1 19.4%, H-4→L+2 2.30%, H-3→L+1 22.0%, H-3→L+2 13.2%, H-2→L+1 2.13%, H-2→L+2 27.6%, H→L +1 2.43%, H→L+2 6.79%
T_{10}	4.817	H-4→L 1.92%, H-4→L+1 3.21%, H-3→L 1.43%, H-3→L+2 4.57%, H-2→L 2.88%, H-2→L+1 5.53%, H-2→L +2 1.36%, H-1→L+2 1.36%, H-1→L+1 1.02%, H-1→L+4 2.79%, H→L+1 54.5%, H→L+2 13.1%, H→L+3 2.54%

Table S6. The singlet (S_1) and triplet (T_n) state transition configurations for the BC dimer.

States	Energy (eV)	Transition configuration (%)
S_1	2.431	H→L 94.5%, H→L+1 1.39%, H→L+4 1.70%
T_1	1.623	H-1→L+4 3.61%, H→L 67.7%, H→L+1 13.3%, H→L+4 1.36%, H→L+6 1.68%
T_2	2.233	H-3→L 2.15%, H-2→L 1.59%, H-1→L 5.71%, H→L 7.73%, H→L+1 62.5%, H→L+2 3.87%, H→L+6 9.19%
T_3	2.313	H-2→L 2.22%, H-1→L 31.1%, H-1→L+1 8.04%, H-1→L+4 2.38%, H→L 2.82%, H→L+3 2.53%, H-1→L+4 36.6%. H→L+7 2.77%
T_4	2.498	H-3→L 1.66%, H-3→L+1 2.53%, H-1→L 13.8%, H-1→L+4 7.26%, H→L 5.82%, H→L+1 8.19%, H→L+4 25.2%, H→L+6 20.1%, H→L+7 2.77%
T_5	2.665	H-3→L 2.82%, H-2→L+1 1.55%, H-1→L 10.5%, H-1→L+1 7.21%, H-1→L+4 5.38%, H-1→L+6 1.36%, H→L 1.49%, H→L+2 1.14%, H→L+3 9.88%, H→L+4 14.3%, H→L+5 3.83%, H→L+6 28.5%, H→L+7 1.52%

T_6	2.747	H-4→L+4 1.02%, H-2→L 13.9%, H-2→L+1 3.93%, H-2→L+4 1.19%, H-1→L+1 11.8%, H-1→L+3 1.94%, H-1→L+4 32.7%, H-1→L+5 3.52%, H-1→L+3 9.88%, H→L+4 14.3%, H→L+5 3.83%, H→L 7.76%, H→L+1 2.73%
T_7	2.784	H-3→L 6.96%, H-3→L+1 6.72%, H-3→L+2 1.29%, H-3→L +7 1.17%, H-2→L 13.4%, H-1→L 16.9%, H-1→L+1 10.3%, H-1→L+4 10.9%, H-1→L+6 4.08%, H→L+6 5.98%
T_8	2.887	H-2→L 8.47%, H-2→L+1 3.00%, H-1→L 2.09%, H→L 1.87%, H→L+1 4.28%, H→L+2 71.4%
T_9	2.917	H-3→L 3.82%, H-3→L+1 1.41%, H-2→L 16.6%, H-2→L+1 9.73%, H-1→L+1 20.1%, H-1→L+4 6.45%, H→L+2 13.0%, H→L+3 1.13%, H→L+6 12.1%
T_{10}	3.123	H-1→L+5 1.04%, H-1→L+1 1.16%, H→L+3 55.9%, H→L+4 1.24%, H→L+5 23.7%, H→L+6 2.94%

Table S7. The singlet (S_1) and triplet (T_n) state transition configurations for the BC dimer.

States	Energy (eV)	Transition configuration (%)
S_1	1.621	H→L 98.8%
T_1	1.110	H-2→L+7 1.66%, H→L+1 13.7%, H→L+2 12.9%, H→L+3 11.8%, H→L+4 47.4%, H→L+7 4.96%
T_2	1.493	H-3→L+7 1.47%, H-2→L+7 4.02%, H→L 22.3%, H→L+2 15.1%, H→L+3 3.14%, H→L+5 7.25%, H→L+6 5.16%, H→L+7 35.3%
T_3	1.569	H-3→L+7 1.73%, H-2→L+7 3.45%, H→L 13.8%, H→L+3 3.42%, H→L+5 27.1%, H→L+6 13.9%, H→L+7 28.3%.
T_4	1.648	H→L 61.1%, H→L+1 1.25%, H→L+2 7.37%, H→L+5 13.9%, H→L+6 10.4%, H→L+7 1.11%, H→L+8 29.9%
T_5	1.725	H-1→L+8 1.21%, H→L+1 36.8%, H→L+2 7.25%, H→L+4 1.47%, H→L+5 13.8%, H→L+7 1.74%, H→L+8 29.9%
T_6	1.891	H-1→L+8 1.39%, H→L+1 46.5%, H→L+3 1.74%, H→L+4 7.76%,

		H→L+5 5.51%, H→L+6 2.62%, H→L+8 30.3%
T_7	2.017	H→L+2 54.7%, H→L+3 13.0%, H→L+4 9.77%, H→L +5 1.64%, H→L+6 6.11%, H→L+7 2.56%, H→L+6 8.57%
T_8	2.202	H→L+3 62.2%, H→L+4 27.5%, H→L+7 4.84%, H→L+9 1.61%
T_9	2.258	H-3→L+5 2.23%, H-3→L+6 1.59%, H-2→L+1 5.86%, H-2→L+2 9.01%, H-2→L+3 7.67%, H-2→L+4 26.1%, H-1→L+1 4.28%, H-1→L+2 5.39%, H-1→L+3 2.83%, H-1→L+4 10.5%, H→L+3 1.09%, H→L+9 8.76%
T_{10}	2.368	H-2→L+1 1.62%, H-2→L+2 1.17%, H-2→L+4 10.2%, H-2→L+7 14.8%, H-2→L+8 1.15%, H-1→L+1 10.8%, H-1→L+2 9.13%, H-1→L+3 7.27%, H-1→L+4 15.3%, H-1→L+7 1.83%, H→L+4 1.15%, H→L+7 1.36%

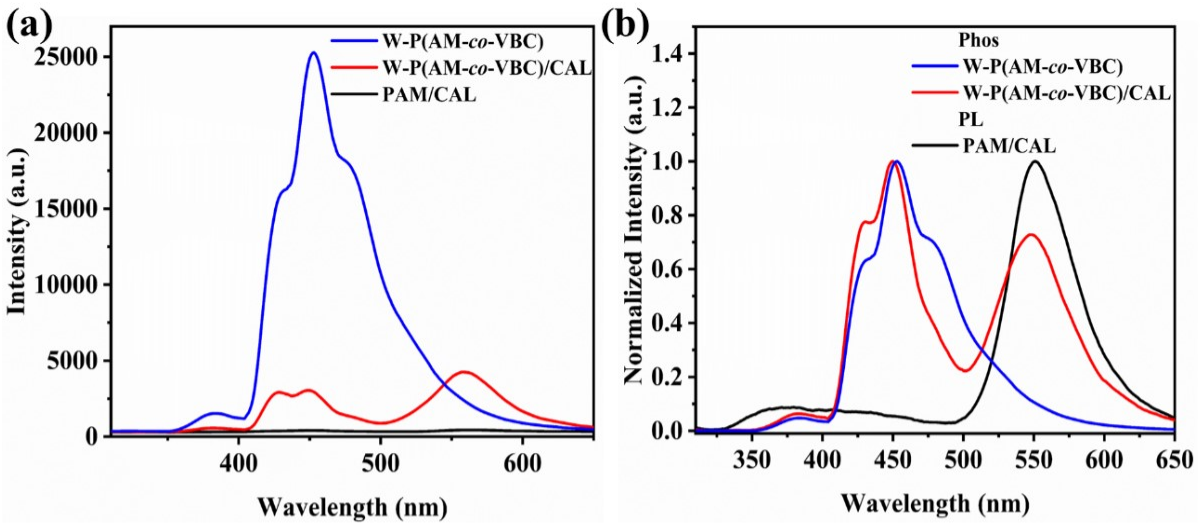

Fig. S13. (a) Phosphorescence spectra of W-P(AM-*co*-VBC), W-P(AM-*co*-VBC)/CAL and PAM/CAL (λ_{ex} = 245 nm, delay time = 10 ms). (b) Normalized phosphorescence spectra of W-P(AM-*co*-VBC), W-P(AM-*co*-VBC)/ CAL and steady-state PL spectrum of PAM/CAL.

Table S8. Delayed fluorescence quantum yield (QY), phosphorescence lifetime (τ) and energy transfer efficiency (η_{ET}) of W-P(AM-*co*-VBC)/CAL with different weight ratios at 442 nm.

weight ratio	QY (%)	τ (ms)	η_{ET}
1000:0.11	12.60	4104	12.01%
1000:0.22	14.28	3873	16.96%
1000:0.66	20.57	3689	20.90%
1000:1.1	27.49	3510	24.74%
1000:1.54	29.33	3383	27.47%
1000:1.98	29.63	3134	32.80%

$\eta_{ET} = (\tau_0-\tau)/\tau_0$, where τ_0 is the original lifetime (4664 ms) of W-P(AM-*co*-VBC), and τ is the new lifetime of W-P(AM-*co*-VBC)/CAL with different weight ratios.

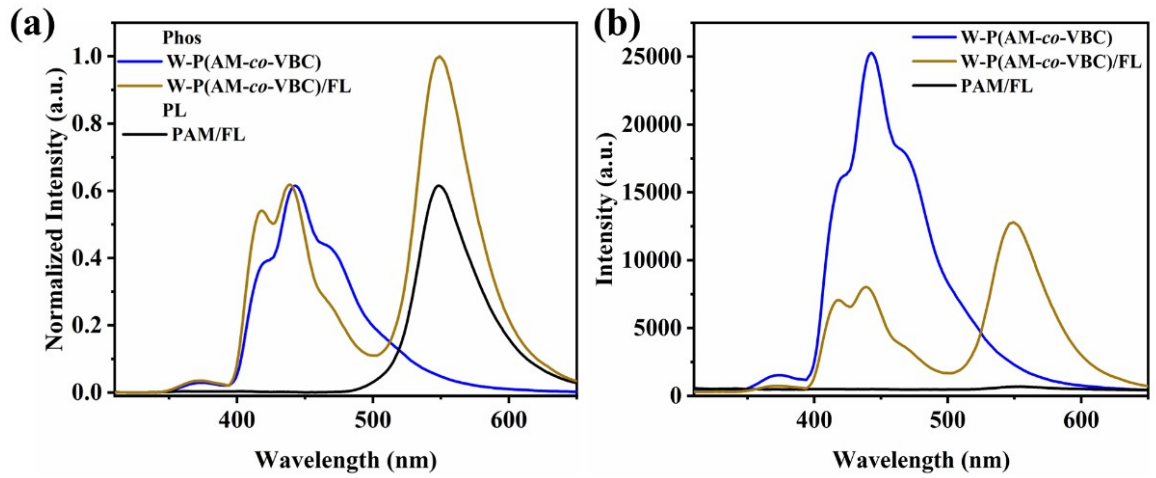

Fig. S14. (a) Normalized phosphorescence spectra of W-P(AM-*co*-VBC), W-P(AM-*co*-VBC)/FL and steady-state PL spectrum of PAM/FL. (b) Phosphorescence spectra of W-P(AM-*co*-VBC), W-P(AM-*co*-VBC)/FL and PAM/FL (λ_{ex} = 245 nm, delay time = 10 ms).

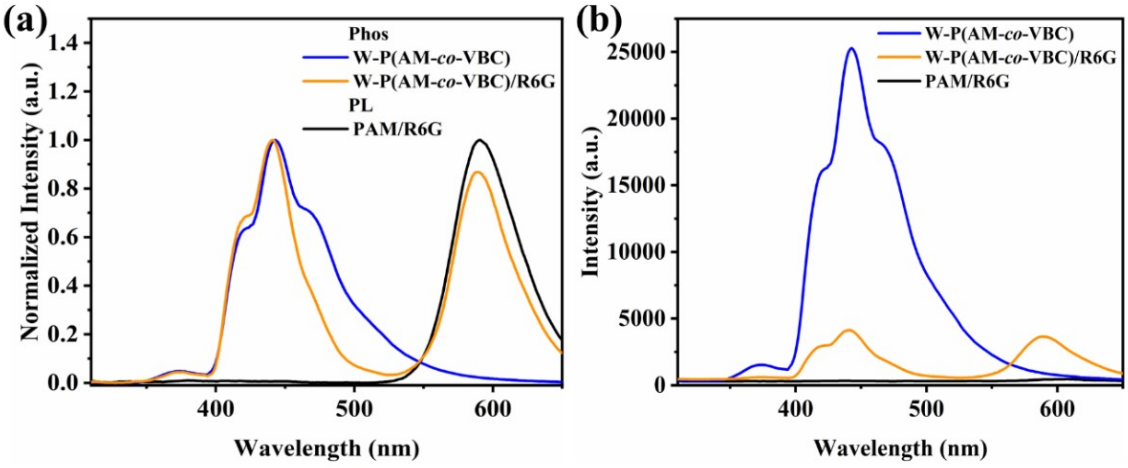

Fig. S15. (a) Normalized phosphorescence spectra of W-P(AM-*co*-VBC), W-P(AM-*co*-VBC)/R6G and steady-state PL spectrum of PAM/R6G. (b) Phosphorescence spectra of W-P(AM-*co*-VBC), W-P(AM-*co*-VBC)/R6G and PAM/R6G (λ_{ex} = 245 nm, delay time = 10 ms).

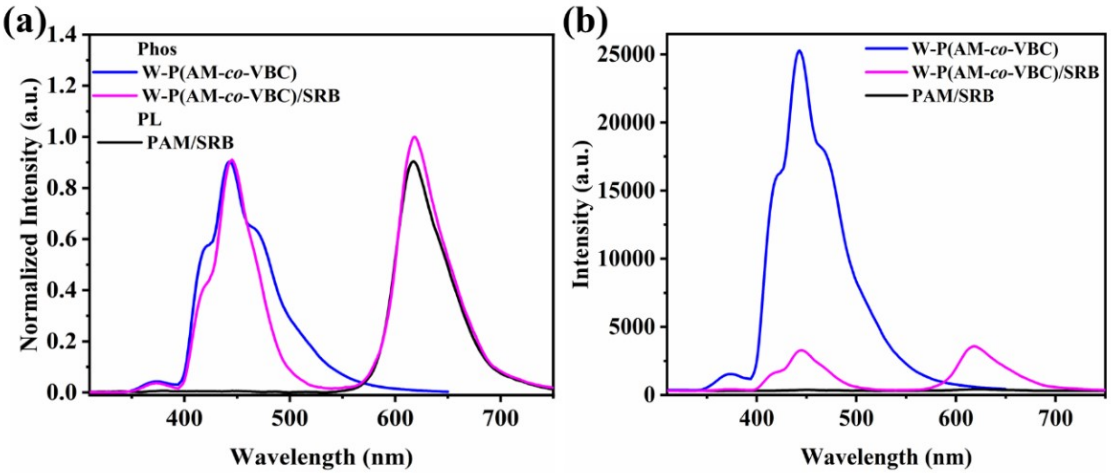

Fig. S16. (a) Normalized phosphorescence spectra of W-P(AM-*co*-VBC), W-P(AM-*co*-VBC)/SRB and steady-state PL spectrum of PAM/SRB. (b) Phosphorescence spectra of W-P(AM-*co*-VBC), W-P(AM-*co*-VBC)/SRB and PAM/SRB (λ_{ex} = 245 nm, delay time = 10 ms).

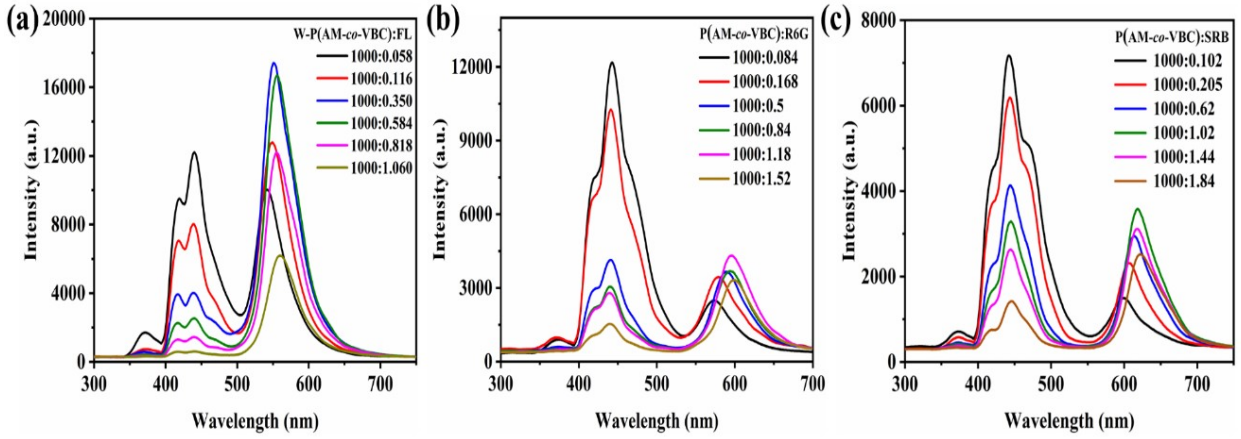

Fig. S17. Phosphorescence spectra of W-P(AM-*co*-VBC)/FL (a), W-P(AM-*co*-VBC)/R6G (b), and W-P(AM-*co*-VBC)/SRB (c).

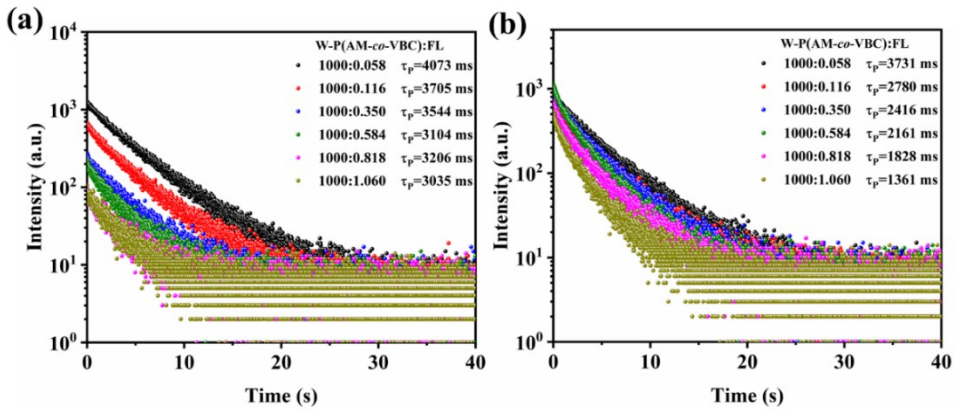

Fig. S18. (a) Time-resolved decay curves of W-P(AM-*co*-VBC)/FL at 442 nm (λ_{ex} = 245 nm). (b) Time-resolved decay curves of W-P(AM-*co*-VBC)/FL at 548 nm (λ_{ex} = 245 nm).

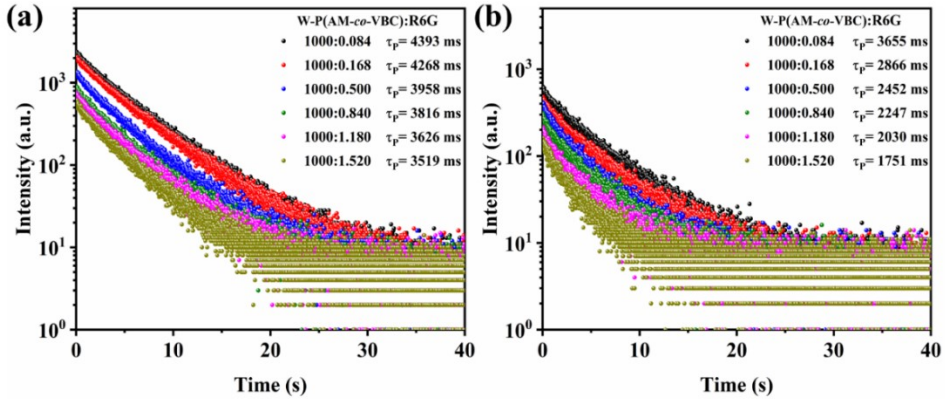

Fig. S19. (a) Time-resolved decay curves of W-P(AM-*co*-VBC)/R6G at 442 nm (λ_{ex} = 245 nm). (b) Time-resolved decay curves of W-P(AM-*co*-VBC)/R6G at 590 nm (λ_{ex} = 245 nm).

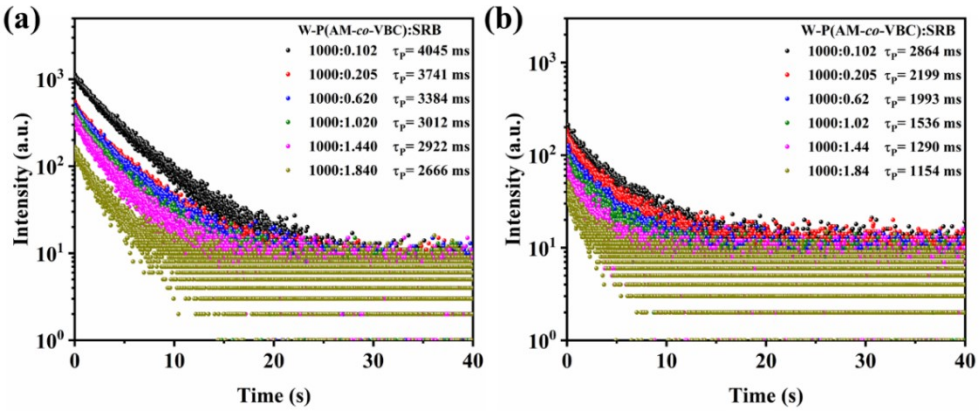

Fig. S20. (a) Time-resolved decay curves of W-P(AM-*co*-VBC)/SRB at 442 nm (λ_{ex} = 245 nm). (b) Time-resolved decay curves of W-P(AM-*co*-VBC)/SRB at 618 nm (λ_{ex} = 245 nm).

Table S9. Delayed fluorescence quantum yield (QY), phosphorescence lifetime (τ) and energy transfer efficiency (η_{ET}) of W-P(AM-*co*-VBC)/FL with different weight ratios at 442 nm..

weight ratio	QY (%)	τ (ms)	η_{ET}
1000:0.058	15.04	4073	12.67%
1000:0.116	23.55	3705	20.56%
1000:0.350	43.13	3544	24.01%
1000:0.584	51.66	3404	27.02%
1000:0.818	49.89	3206	31.26%
1000:1.060	55.22	3035	34.93%

$\eta_{ET} = (\tau_0-\tau)/\tau_0$, where τ_0 is the original lifetime (4664 ms) of W-P(AM-*co*-VBC), and τ is the new lifetime of W-P(AM-*co*-VBC)/FL with different weight ratios.

Table S10. Delayed fluorescence quantum yield (QY), phosphorescence lifetime (τ) and energy transfer efficiency (η_{ET}) of W-P(AM-*co*-VBC)/R6G with different weight ratios at 442 nm..

weight ratio	QY (%)	τ (ms)	η_{ET}
1000:0.084	8.88	4393	5.81%
1000:0.168	14.69	4268	8.49%
1000:0.50	23.15	3958	15.14%
1000:0.84	31.28	3816	18.18%
1000:1.18	32.76	3626	22.26%
1000:1.52	31.61	3519	24.55%

$\eta_{ET} = (\tau_0-\tau)/\tau_0$, where τ_0 is the original lifetime (4664 ms) of W-P(AM-*co*-VBC), and τ is the new lifetime of W-P(AM-*co*-VBC)/R6G with different weight ratios.

Table S11. Delayed fluorescence quantum yield (QY), phosphorescence lifetime (τ) and energy transfer efficiency (η_{ET}) of W-P(AM-*co*-VBC)/SRB with different weight ratios at 442 nm..

weight ratio	QY (%)	τ (ms)	η_{ET}
1000:0.102	12.79	4045	13.27%
1000:0.205	20.23	3741	19.79%
1000:0.620	37.67	3384	27.44%
1000:1.020	40.86	3012	35.42%
1000:1.440	45.39	2922	37.35%
1000:1.840	46.72	2666	42.84%

$\eta_{ET} = (\tau_0-\tau)/\tau_0$, where τ_0 is the original lifetime (4664 ms) of W-P(AM-*co*-VBC), and τ is the new lifetime of W-P(AM-*co*-VBC)/SRB with different weight ratios.

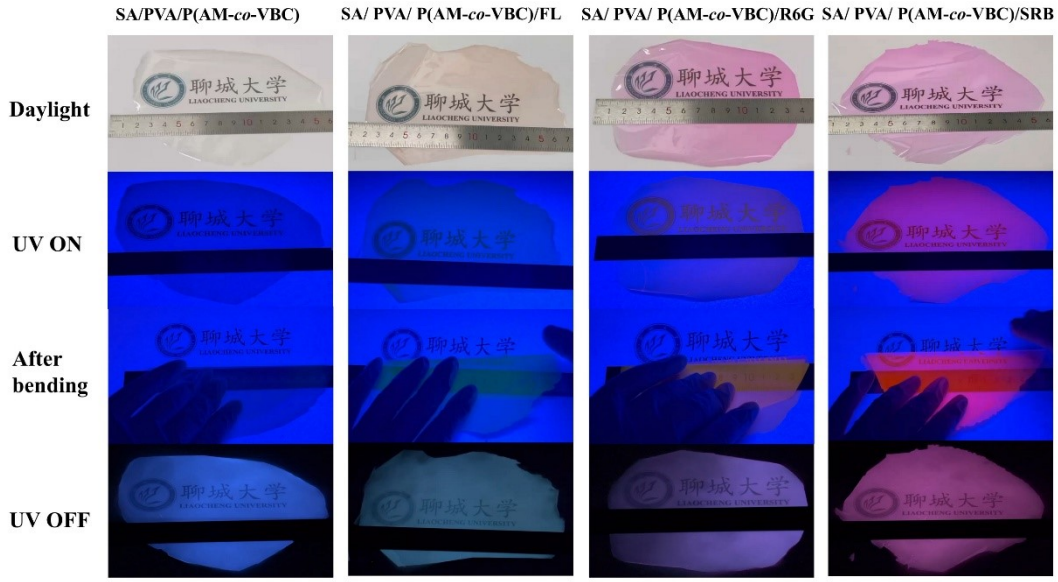

Fig. S21. Photographs of flexible multicolor RTP films.

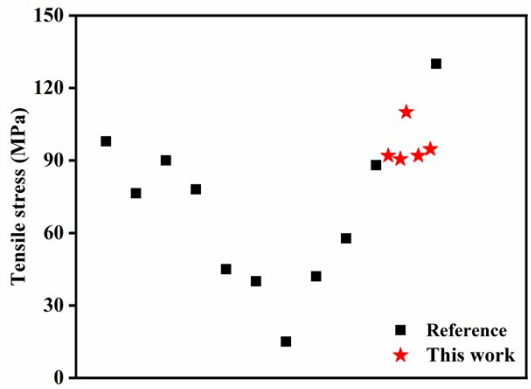

Fig. S22. Comparison of tensile stress between the prepared SA-based flexible RTP films and some reported polymer-based RTP films.[1-8]

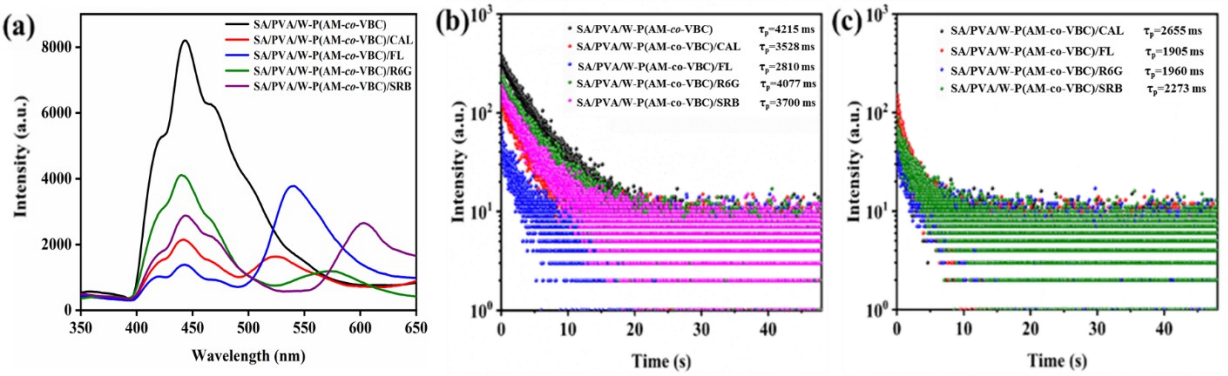

Fig. S23. (a) Phosphorescence spectra of SA-based flexible RTP films (λ_{ex} = 245 nm, delayed time = 10 ms). (b) Time-resolved decay curves of SA-based flexible RTP films at 442 nm (λ_{ex} = 245 nm). (c) Time-resolved decay curves of SA-based flexible RTP films at the emission peaks of energy acceptors (λ_{ex} = 245 nm).

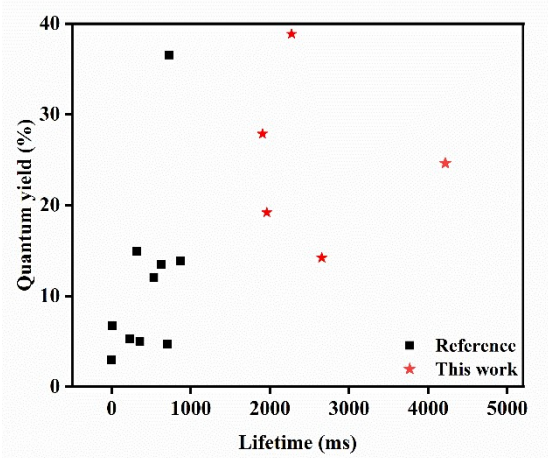

Fig. S24. Comparison of phosphorescence lifetime and QY between the prepared SA-based flexible RTP films and some reported polymer-based RTP films.[1-3,9-15]

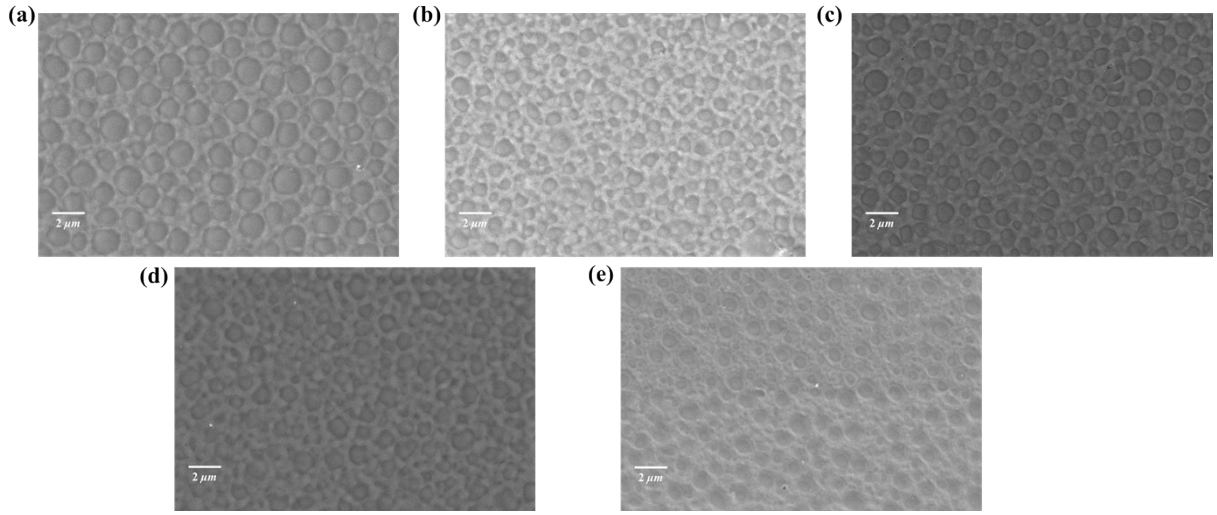

Fig. S25. FESEM micrographs of SA/PVA/W-P(AM-*co*-VBC) (a), SA/PVA/W-P(AM-*co*-VBC)/CAL (b), SA/PVA/W-P(AM-*co*-VBC)/FL (c), SA//PVA/W-P(AM-*co*-VBC)/R6G (d), and SA/PVA/W-P(AM-*co*-VBC)/SRB (e).

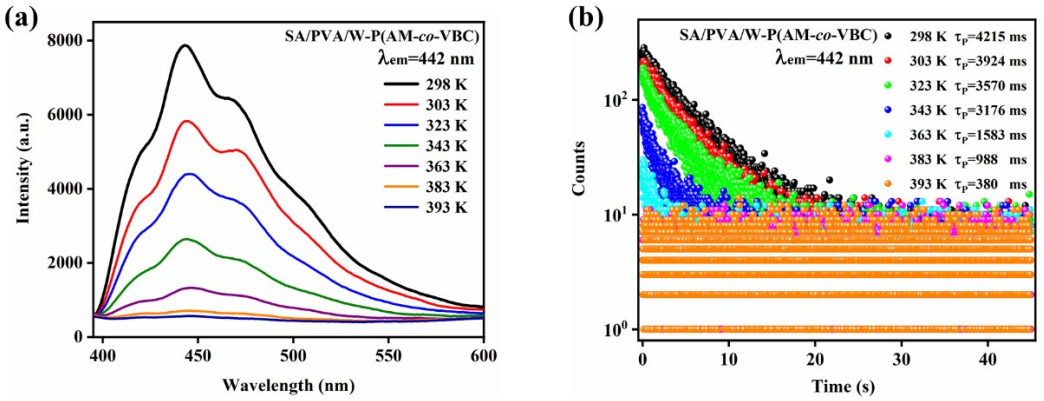

Fig. S26. (a) Phosphorescence spectra of SA/PVA/W-P(AM-*co*-VBC) at different temperatures. (b) Time-resolved decay curves of SA/PVA/W-P(AM-*co*-VBC) at different temperatures.

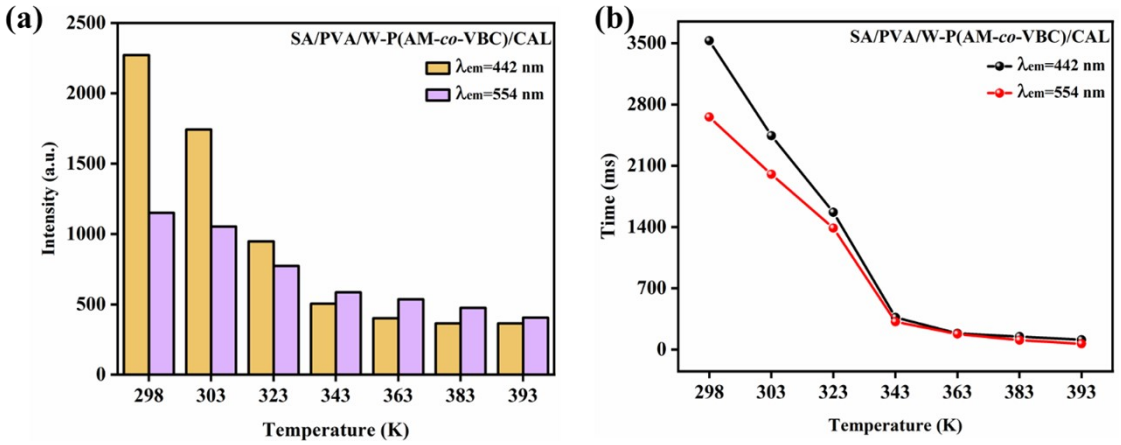

Fig. S27. Phosphorescence intensity histogram (a) and phosphorescence lifetime trend chart (b) of SA/PVA/W-P(AM-*co*-VBC)/CAL at different temperatures.

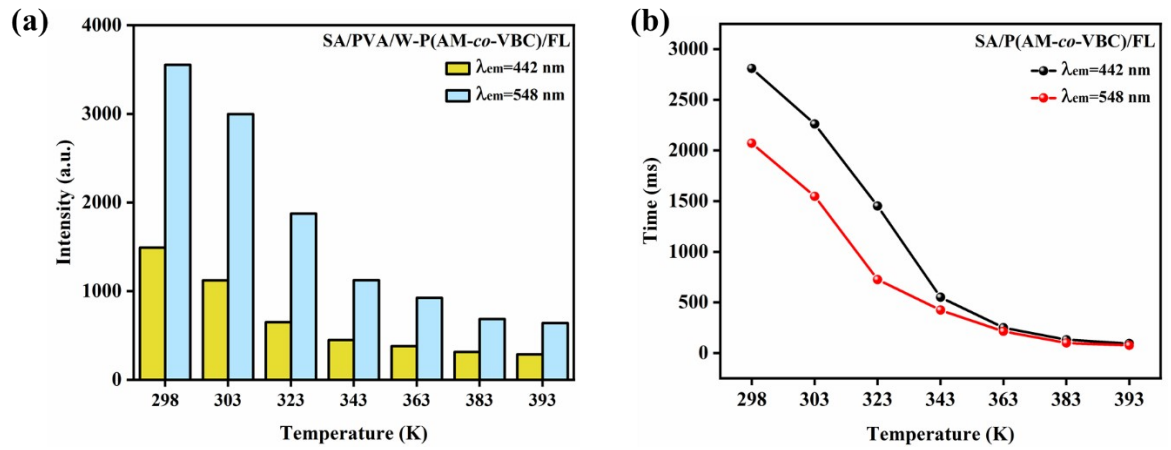

Fig. S28. Phosphorescence intensity histogram (a) and phosphorescence lifetime trend chart (b) of SA/PVA/W-P(AM-*co*-VBC)/FL at different temperatures.

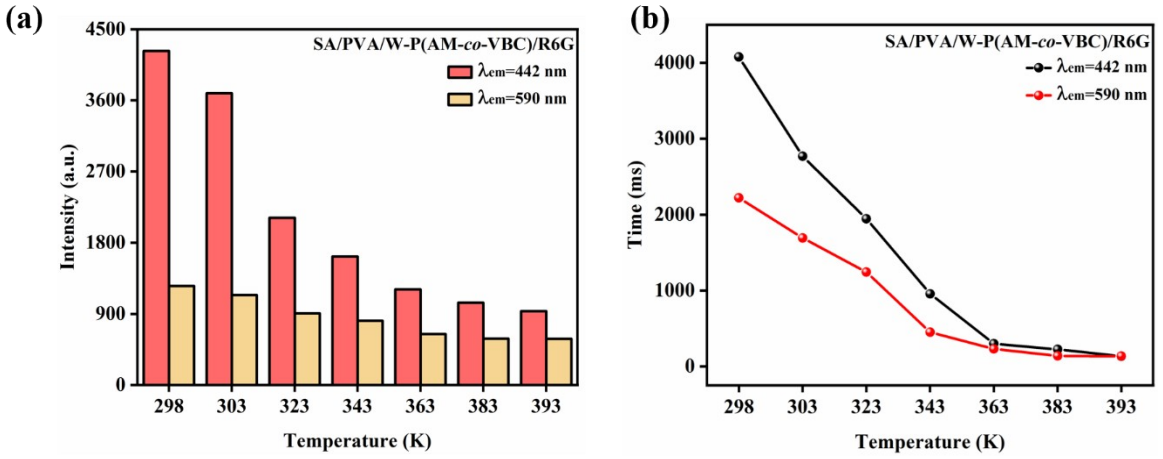

Fig. S29. Phosphorescence intensity histogram (a) and phosphorescence lifetime trend chart (b) of SA/PVA/W-P(AM-*co*-VBC)/R6G at different temperatures.

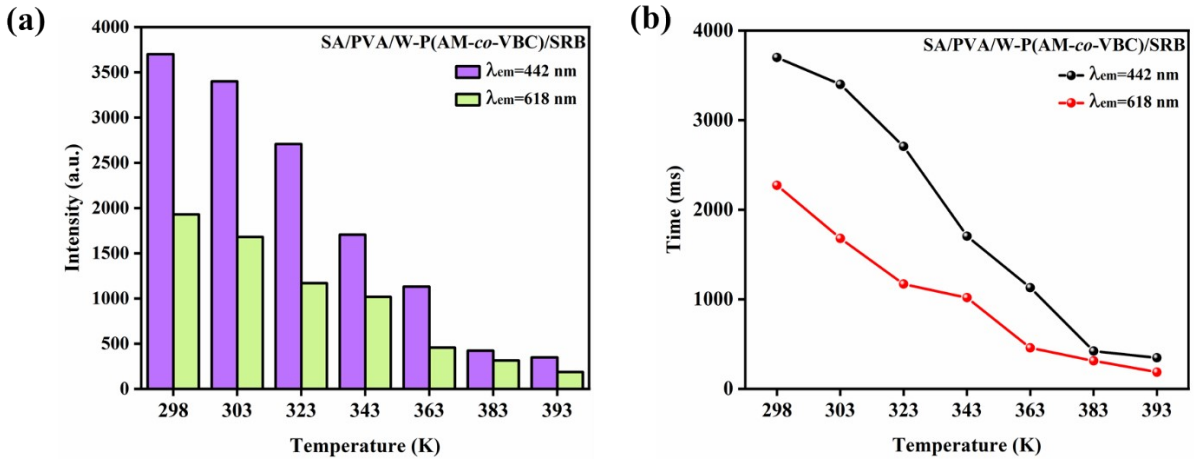

Fig. S30. Phosphorescence intensity histogram (a) and phosphorescence lifetime trend chart (b) of SA/PVA/W-P(AM-*co*-VBC)/SRB at different temperatures.

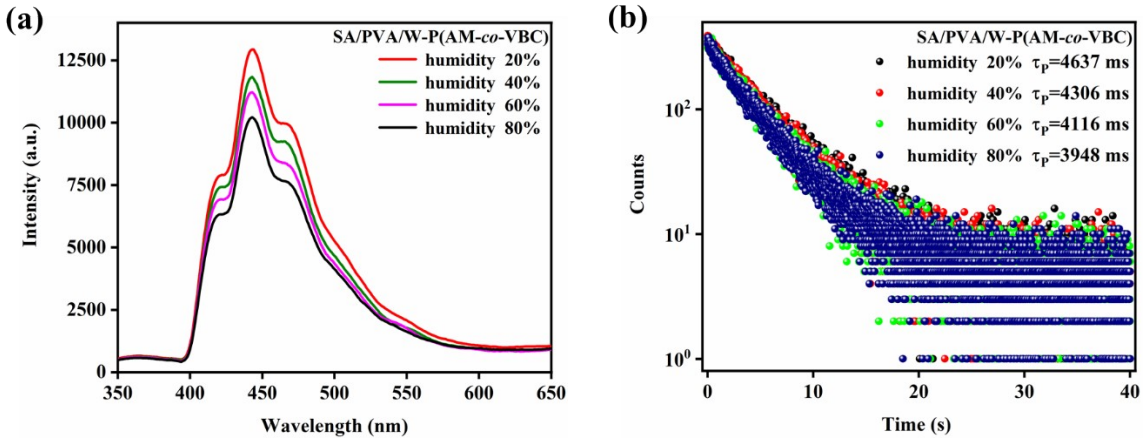

Fig. S31. (a) Phosphorescence spectra of SA/PVA/W-P(AM-*co*-VBC) at different humidity levels. (b) Time-resolved decay curves of SA/PVA/W-P(AM-*co*-VBC) at different humidity levels (λ_{em}=442 nm).

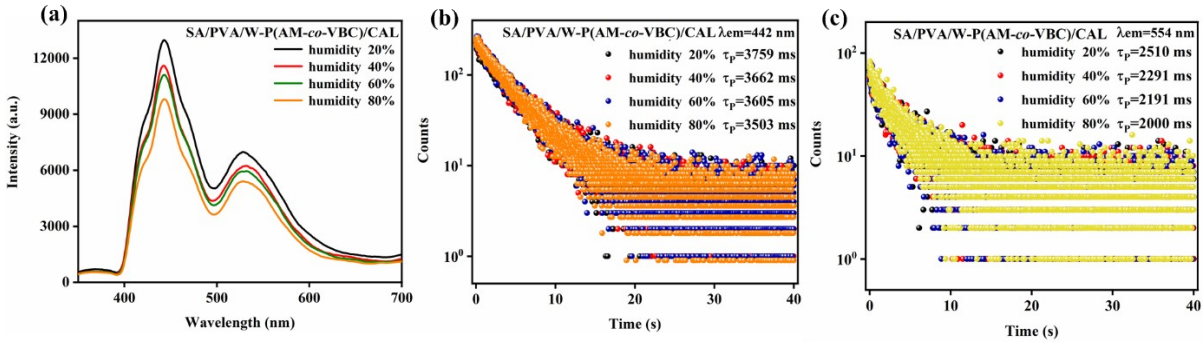

Fig. S32. (a) Phosphorescence spectra of SA/PVA/W-P(AM-*co*-VBC)/CAL at different humidity levels. (b) Time-resolved decay curves of SA/PVA/W-P(AM-*co*-VBC)/CAL at different humidity levels (λ_{em}=442 nm). (c) Time-resolved decay curves of SA/PVA/W-P(AM-*co*-VBC)/CAL at different humidity levels (λ_{em}=554 nm).

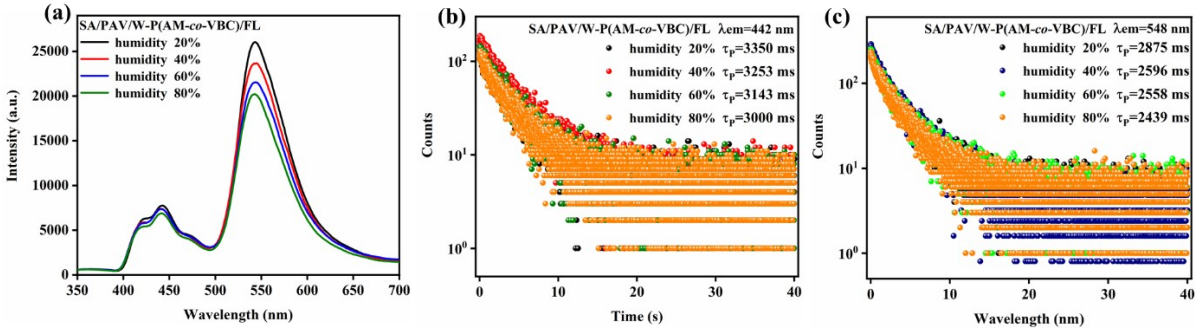

Fig. S33. (a) Phosphorescence spectra of SA/PVA/W-P(AM-*co*-VBC)/FL at different humidity levels. (b) Time-resolved decay curves of SA/PVA/W-P(AM-*co*-VBC)/FL at different humidity levels (λ_{em}=442 nm). (c) Time-resolved decay curves of SA/PVA/W-P(AM-*co*-VBC)/FL at different humidity levels (λ_{em}=548 nm).

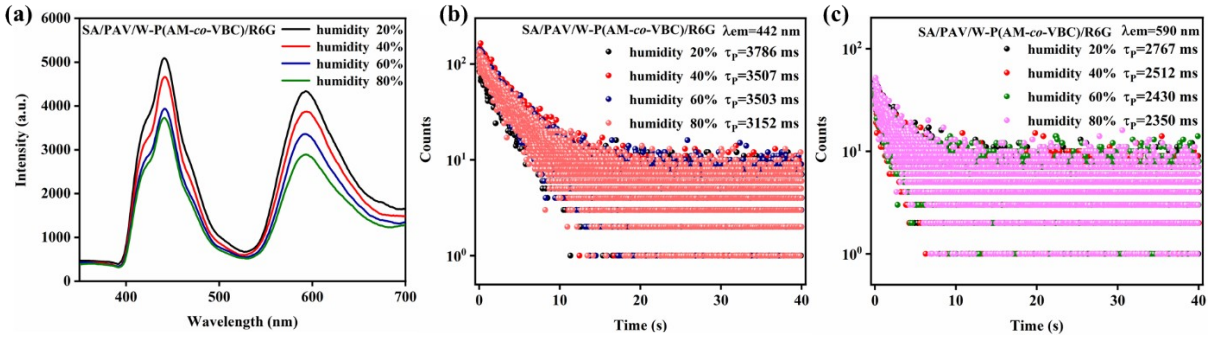

Fig. S34. (a) Phosphorescence spectra of SA/PVA/W-P(AM-*co*-VBC)/R6G at different humidity levels. (b) Time-resolved decay curves of SA/PVA/W-P(AM-*co*-VBC)/R6G at different humidity levels (λ_{em}=442 nm). (c) Time-resolved decay curves of SA/PVA/W-P(AM-*co*-VBC)/R6G at different humidity levels (λ_{em}=590 nm).

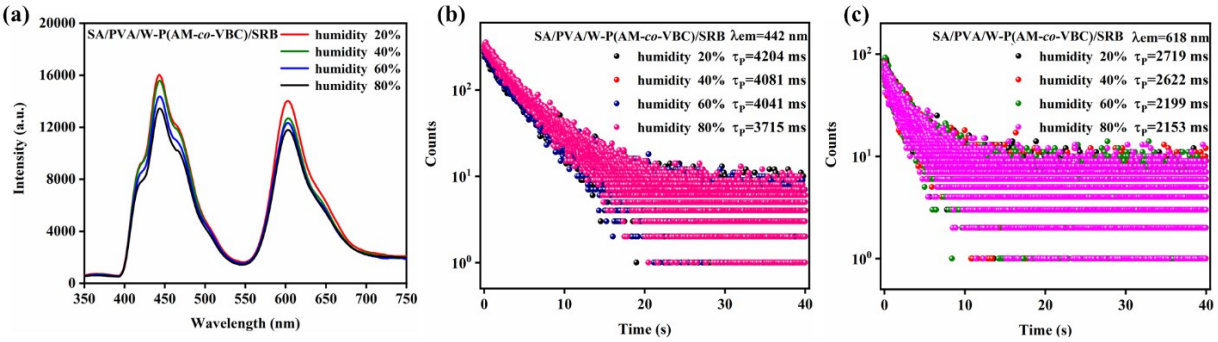

Fig. S35. (a) Phosphorescence spectra of SA/PVA/W-P(AM-*co*-VBC)/R6G at different humidity levels. (b) Time-resolved decay curves of SA/PVA/W-P(AM-*co*-VBC)/R6G at different humidity levels (λ_{em}=442 nm). (c) Time-resolved decay curves of SA/PVA/W-P(AM-*co*-VBC)/R6G at different humidity levels (λ_{em}=618 nm).

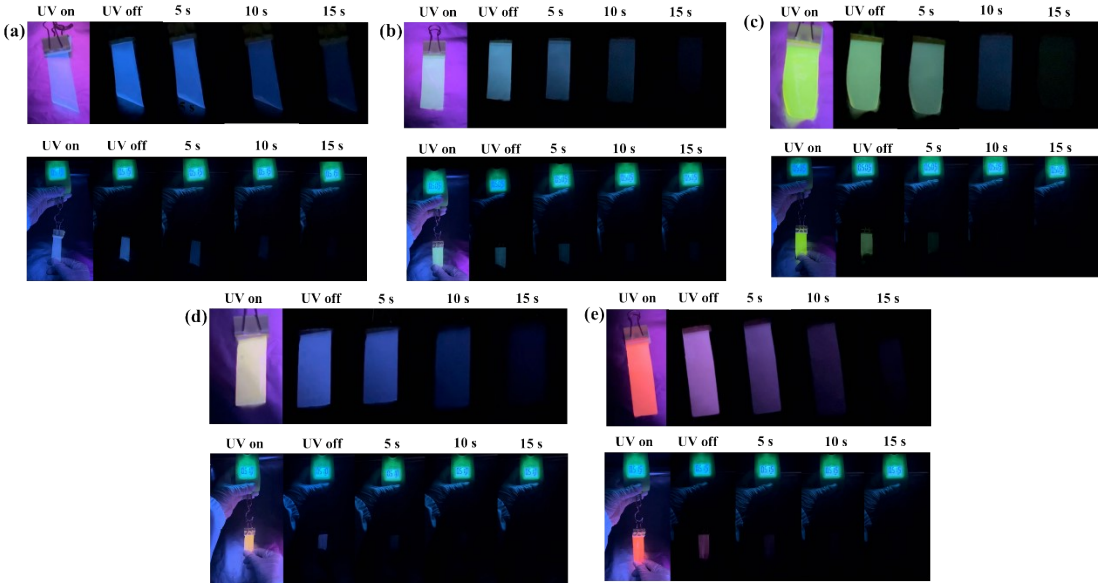

Fig. S36. Photographs of SA/PVA/W-P(AM-*co*-VBC) (a), SA/PVA/W-P(AM-*co*-VBC)/CAL (b), SA/PVA/W-P(AM-*co*-VBC)/FL (c), SA//PVA/W-P(AM-*co*-VBC)/R6G (d), and SA/PVA/W-P(AM-*co*-VBC)/SRB (e) films with and without a tensile force (5 ± 0.05 N) under

254 nm UV light and after ceasing the irradiation.

Reference

[1] P. Li, Y. Yu, J. Zhou, S. Wei, J. Han, X. Li, M. Wei, T. Chen and W. Lu, *Small,* 2025, **21**, e08588.

[2] C. Li, G. Miao, S. Chen and F. Xu, *Adv. Funct. Mater*., 2025, e26407, DOI: 10.1002/adfm.202526407.

[3] W. Ye, T. Cao, Z. Gao, B. Hu, L. Chen and C. Wang, *ACS Appl. Nano. Mater*., 2025, **8**, 7848-7857.

[4] T. Liu, X. Lian, L. Li, X. Peng and T. Kuang, *Polym. Degrad. Stab*., 2020, **171**, 109044.

[5] S. Park, H. Jeon, H. Kim, S. Shin, S. Choy, D. Hwang, J. Koo, J. Jegal, S. Hwang, J. Park and D. Oh, *Nat. Commun*., 2021, **10**, 2601.

[6] S. Zhu, S. Biswas, Z. Qiu, Y. Yue, Q. Fu, F. Jiang and J. Han, *Prog. Mater. Sci*., 2023, **132** 101025.

[7] H. Shu, L. Chen, X. Wu, T. Wang, S. Wang, H. Tong and L. Wang, *J. Mater. Chem. C*., 2022,**10**, 1833-1838.

[8] D. Shahdan, R. Chen, S. Ahmad, F. Zailan and A. Ali, *Polym. Int*., 2018, **67**, 1070-1080.

[9] M. Louis, H. Thomas, M. Gmelch, A. Haft, F. Fries and S. Reineke, *Adv. Mater*., 2019, **31**, 1807887.

[10] S. Sun, L. Ma, J. Wang, X. Ma and H. Tian, *Nat. Sci. Rev*., 2022, **9**, nwab085.

[11] Y. Yao, D. Huang, P. Han, X. Peng, X. He, H. Xu, A. Qin, B. Tang, *ACS Materials Lett.,* 2025, **7**, 133-140.

[12] H. Li, Q. Zhang, H. Zhang, Q. Cui, C. Liu and L. Li, *Colloids Surf. A*., 2024, **689**, 2, 133760.

[13] Y. Yang, Y. Qi, A. Li, Y. Shan, Z. Chen, M. Shan, X. Du, K. Wang, K. Yang, B. Tang and Z. Li, *Adv. Mater.,* 2026, e18840, DOI: 10.1002/adma.202518840.

[14] S. Jia, B. Yang, S. Guo, Y. Zhang, W. Tang and J. Gong, *Small,* 2026, **22**, e10075.

[15] R. Tian, S. Gao, K. Li and C. Lu, *Nat. Commun*., 2023, **14**, 4720.